Hindawi
Shock and Vibration
Volume 2024, Article ID 1842508, 12 pages
https://doi.org/10.1155/2024/1842508

Research Article

An Electromagnetic Load Identification Method Based on the Polynomial Structure Selection Technique

Wengui Mao,[1] **Shixiong Pei**,[1] **Jie Guo**,[1] **Jianhua Li**,[1] **and Buyao Wang**[2]

[1]*Hunan Province Cooperative Innovation Center for Wind Power Equipment and Energy Conversion, College of Mechanical Engineering, Hunan Institute of Engineering, Xiangtan 411104, China*
[2]*Xiangtan Electric Machinery Co., Ltd, Xiangtan 411100, China*

Correspondence should be addressed to Jianhua Li; 07124@hnie.edu.cn

Received 12 June 2023; Revised 25 December 2023; Accepted 8 January 2024; Published 13 January 2024

Academic Editor: Vasudevan Rajamohan

Copyright © 2024 Wengui Mao et al. This is an open access article distributed under the Creative Commons Attribution License, which permits unrestricted use, distribution, and reproduction in any medium, provided the original work is properly cited.

Electromagnetic loads can effectively monitor motor health and improve motor design. Considering the weak correlation of the modal shape and Chebyshev orthogonal polynomial in the space-time independent electromagnetic load identification method, a proposed method combining the polynomial structure selection technique together with limited measured displacement responses is presented, in which an error reduction ratio is used to pick out the significant mode shape matrix and the Chebyshev orthogonal polynomial. The time-history function of the electromagnetic load is reconstructed by combining the significant mode shape matrix and the identified concentrated load through modal transformation, and the corresponding spatial distribution function is fitted by the significant Chebyshev orthogonal polynomial. Eventually, a comparative numerical study considering the selection of significant components and measurement noise is carried out to prove the effectiveness of the presented method.

1. Introduction

Energy problems and the vibration and noise problems of wind turbines during operation have received widespread attention from scholars around the world [1–3]. Particularly, the radial electromagnetic load coming from the air-gap eccentricity variation pattern with time is the main factor of noise and vibration [4–6]. Its accurate identification has become a hot research topic for promoting the motor performance due to its assistance for vibration prediction, structural design, and health monitoring [7–9]. However, the electromagnetic load coming from the air-gap eccentricity occurring during motor operation due to disturbances from external excitations is distributed dynamic load, and its identification (or reconstruction) is the second inverse problem in structural dynamic analysis [10], which is the process of reconstructing the loads applied on the structure with the structural dynamic model and structural response information [11–14]. Different from the concentrated dynamic load, the representation of the electromagnetic load requires variables in both the time domain and the space domain. Consequently, the scale and difficulty of the calculation are greatly increased.

The subsistent investigates for distributed dynamic loads identification [15, 16] are mainly under the consideration of the multipoint concentrated dynamic load equivalented and basic functions fitted. The spatial distribution function may be fitted by linearly independent basis functions according to the generalized orthogonal domain theory [17]. Wang et al. [10] showed that the complex nonlinear spatial distribution function can also be effectively fitted by Chebyshev orthogonal polynomials. Jiang et al. [18] reconstructed the space-time coupling distributed load combining modal transformation together with orthogonal decomposition. Mao et al. [19] reconstructed the space-time independent electromagnetic load combining the equivalented concentrated dynamic load with basis function fitting. Zhang et al. [12] transformed distributed dynamic loads to equivalented concentrated loads acting on appropriate locations according to the strain modal theory. Li et al. [20] used the Tikhonov regularization scheme to identify the ratio of orthogonal polynomials and found that only enough

measuring points are needed to meet the accuracy of distributed load identification. However, some shortcomings still existed in the methods abovementioned; the weak correlation of modal shape and basis function terms will cause the serious ill-posedness in time-history reconstruction and spatial distribution function fitting due to the determination of the modal shape and the basis function terms.

In this paper, a polynomial selection technique [20] is introduced to improve the ill-posedness problem, in which the contribution rate of each component is calculated by the error reduction ratio and the components with the small contribution rate are eliminated. The rest of this paper is organized as follows. Section 2 briefly introduces the electromagnetic load identification problem. In Section 3, the electromagnetic load reconstruction based on the polynomial selection technique is introduced in detail. In Section 4, a comparative numerical example is used to verify the effectiveness. In Section 5, some conclusions are briefly summarized.

2. Problem Statement

2.1. Electromagnetic Load. The authors in reference [21] show that the electromagnetic load presents the characteristics of space-time independence. Its spatial characteristic is mainly caused by the air-gap eccentricity e (as shown in Figure 1), which is continuous distribution function changing with the spatial domain; its time characteristics are derived from the time-varying mechanical vibration frequency. Therefore, the electromagnetic load shown in the following equation is composed of space-time independent functions, namely, the time-history function $l(t)$ and the spatial distribution function $e(z)$, independently.

$$\mathbf{F}(e,t) = e(z)l(t), \tag{1}$$

where z and t, respectively, denote the variables in the space-time domain.

2.2. The Electromagnetic Load Identification Method. The electromagnetic load can be transformed into a series of concentrated dynamic loads, which have the same time-history form at each action point. Therefore, the dynamic differential equation [19] of the wind turbine rotor under the electromagnetic load can be similar to the dynamic differential equation under the concentrated dynamic load, expressed as shown in the following equation:

$$\mathbf{M}\ddot{\mathbf{q}} + \mathbf{C}\dot{\mathbf{q}} + \mathbf{K}\mathbf{q} = \mathbf{F}(e,t), \tag{2}$$

where $\ddot{\mathbf{q}}$, $\dot{\mathbf{q}}$, and $\mathbf{q}$, respectively, denote the acceleration, velocity, and displacement vector of the wind turbine rotor, and $\mathbf{M}$, $\mathbf{K}$, and $\mathbf{C}$, respectively, denote the mass, stiffness, and damping matrix of the wind turbine rotor.

Performing modal transformation using the mode shape matrix $\mathbf{\Phi}$ and $\mathbf{q} = \mathbf{\Phi}\mathbf{q}^d$ for equation (2), the kinetic equation (2) is thus transferred as

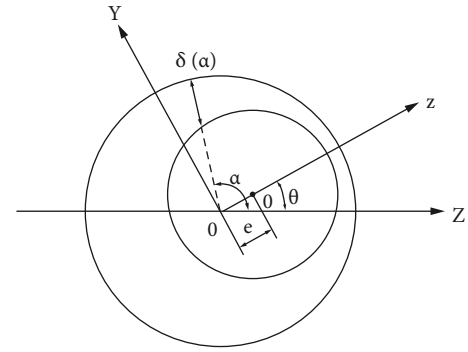

Figure 1: Air-gap eccentricity of the wind turbine rotor.

$$\mathbf{M}^d\ddot{\mathbf{q}}^d + \mathbf{C}^d\dot{\mathbf{q}}^d + \mathbf{K}^d\mathbf{q}^d = \mathbf{F}^d(e,t), \tag{3}$$

where $\mathbf{M}^d = \mathbf{\Phi}^T\mathbf{M}\mathbf{\Phi}$, $\mathbf{K}^d = \mathbf{\Phi}^T\mathbf{K}\mathbf{\Phi}$, and $\mathbf{C}^d = \mathbf{\Phi}^T\mathbf{C}\mathbf{\Phi}$, respectively, denote the modal mass, modal stiffness, and modal damping matrix of the wind turbine rotor. $\mathbf{q}^d$ and $\mathbf{F}^d(e,t)$, respectively, represent the modal displacement vector and the modal electromagnetic load in the modal space.

The modal electromagnetic load $\mathbf{F}^d(e,t)$ is shown in the following equation:

$$\mathbf{F}^d(e,t) = \mathbf{\Phi}^T e(z)l(t) = \begin{bmatrix} c_1 \\ c_2 \\ \vdots \\ c_N \end{bmatrix} l(t) = \begin{bmatrix} p^{d(1)}(t) \\ p^{d(2)}(t) \\ \vdots \\ p^{d(N)}(t) \end{bmatrix}, \tag{4}$$

where $p^{d(i)}(t)$ is the i-th order modal electromagnetic load; $i = 1, 2, 3, \cdots, N$; N is the order of wind turbine rotor; and c_i is a constant.

Equation (4) shows that there are same form and different amplitudes' coefficient c_i between $\mathbf{F}^d(e,t)$ and $l(t)$ and the time-history can be replaced by an assumed-order mode electromagnetic load. Then, the electromagnetic load expression as shown in equation (1) can expressed as shown in the following equation:

$$\begin{aligned} \mathbf{F}(e,t) &= e(z)l(t) = c_i^{-1}e(z)c_i l(t) \\ &= f(z)p^{d(i)}(t) = f(z)s(t), \end{aligned} \tag{5}$$

where $s(t) = p^{d(i)}(t) = c_i l(t)$ and $f(z) = c_i^{-1}e(z)$. Therefore, as long as the assumed-order mode electromagnetic load $s(t)$ and the fitting spatial function $f(z)$ are identified, the electromagnetic load can be reconstructed.

2.2.1. The Time-History Function Identification. Equation (5) shows that the time-history function can be replaced by the modal electromagnetic load. However, it is more difficult to reconstruct the modal load [22] than the concentrated dynamic load in the time domain based on the Green's kernel function method because there must be enough modal orders and the modal response extracted difficultly in the solution process. In this paper, first, the equivalent concentrated dynamic load $\mathbf{F}$ in the acting region is obtained

by combining the conventional load identification method with the time-domain displacement response, as shown in equation (6) [23], and then the modal transformation $\mathbf{F} = \mathbf{\Phi}^T\mathbf{F}$ is carried out to transform the concentrated dynamic load $\mathbf{F}$ into the modal load $\mathbf{F}^d$.

$$\begin{Bmatrix} \mathbf{q}_1 \\ \mathbf{q}_2 \\ \vdots \\ \mathbf{q}_k \end{Bmatrix} = \begin{bmatrix} \mathbf{G}_{11} & \mathbf{G}_{12} & \cdots & \mathbf{G}_{1n} \\ \mathbf{G}_{21} & \mathbf{G}_{22} & \cdots & \mathbf{G}_{2n} \\ \vdots & \vdots & \ddots & \vdots \\ \mathbf{G}_{k1} & \mathbf{G}_{k2} & \cdots & \mathbf{G}_{kn} \end{bmatrix} \begin{Bmatrix} \mathbf{F}_1 \\ \mathbf{F}_2 \\ \vdots \\ \mathbf{F}_n \end{Bmatrix}, \tag{6}$$

where k and n, respectively, refer to the number of the measured response node and the concentrated load node; $\mathbf{q}_k$ represents the k-th measured response; $\mathbf{F}_n$ represents the n-th concentrated dynamic load; and $\mathbf{G}_{kn}$ represents the Green's function matrix.

2.2.2. Spatial Distribution Function Reconstruction. If the generalized Chebyshev polynomial basis function [24] is selected as the fitting function of $f(z)$, then equation (5) is rewritten as shown in the following equation:

$$\mathbf{F}^d(e,t) = f(z)s(t) = s(t)\sum_{i=1}^{m} a_i\mathbf{R}_i, \tag{7}$$

where $\mathbf{R}_i$ and a_i, respectively, denote the i-th generalized Chebyshev polynomial basis function and coefficient; and m denotes the total number of terms of generalized Chebyshev polynomial basis function.

The generalized Chebyshev polynomial basic functions are discretized and equivalent to limited concentrated load nodes, then the electromagnetic load may be equivalent to a series of concentrated dynamic loads on corresponding concentrated nodes, which can be represented as shown in the following equation:

$$\begin{cases} F_1 = (a_1r_{11} + a_2r_{12} + \cdots + a_mr_{1m})s(t), \\ F_2 = (a_1r_{21} + a_2r_{22} + \cdots + a_mr_{2m})s(t), \\ \cdots, \\ F_n = (a_1r_{n1} + a_2r_{n2} + \cdots + a_mr_{nm})s(t), \end{cases} \text{or}$$
$$\begin{bmatrix} F_1 \\ F_2 \\ \vdots \\ F_n \end{bmatrix} = \begin{bmatrix} r_{11} & r_{12} & \cdots & r_{1m} \\ r_{21} & r_{22} & \cdots & r_{2m} \\ \vdots & \vdots & \ddots & \vdots \\ r_{n1} & r_{n2} & \cdots & r_{nm} \end{bmatrix} \begin{bmatrix} a_1 \\ a_2 \\ \vdots \\ a_m \end{bmatrix} s(t). \tag{8}$$

For the equivalent concentrated dynamic load and the modal electromagnetic load, according to the modal relationship $\mathbf{F}^d(e,t) = \mathbf{\Phi}^T\mathbf{F}(e,t)$, the relationship can be shown as follows:

$$\begin{bmatrix} F_1 \\ F_2 \\ \vdots \\ F_n \end{bmatrix} = \mathbf{\Psi}^{-1} \begin{bmatrix} F_1^d \\ F_2^d \\ \vdots \\ F_n^d \end{bmatrix} = \mathbf{\Psi}^{-1} \begin{bmatrix} \lambda_1 \\ \lambda_2 \\ \vdots \\ \lambda_n \end{bmatrix} s(t). \tag{9}$$

Comparing equation (8) with equation (9),

$$\begin{bmatrix} \lambda_1 \\ \lambda_2 \\ \vdots \\ \lambda_n \end{bmatrix} = \mathbf{\Psi} \begin{bmatrix} r_{11} & r_{12} & \cdots & r_{1m} \\ r_{21} & r_{22} & \cdots & r_{2m} \\ \vdots & \vdots & \ddots & \vdots \\ r_{n1} & r_{n2} & \cdots & r_{nm} \end{bmatrix} \begin{bmatrix} a_1 \\ a_2 \\ \vdots \\ a_m \end{bmatrix} \text{or } \boldsymbol{\lambda} = \mathbf{\Psi}\mathbf{r}_i\mathbf{a}, \tag{10}$$

where $\mathbf{\Psi}$ represents the local mode shape matrix with n rows and n columns, which is extracted from the N rows' and N columns' mode shape matrix $\mathbf{\Phi}$ of the wind turbine rotor; λ_j represents the ratio between the modal load F_j^d on j-th equivalent concentrated load node with $s(t)$; r_{ij} represents the equivalent amplitude coefficients solved through the equivalent nodal load method [25]; and fitting $f(z)$ is transformed into the solution of a_i.

In summary, the main factors affecting the identification of the electromagnetic load are the selection of the local mode shape matrix $\mathbf{\Psi}$ and Chebyshev orthogonal polynomial terms. With the increase of modal natural frequency, in fact, not all orders have the same contribution to the equivalent concentrated load in equation (9), and the coefficients of basic functions a_i in equation (10) is affected by the effective term of Chebyshev orthogonal polynomial which produces the equivalent amplitude coefficient r_{ij}. By selecting an effective mode shape matrix and eliminating the weakly correlated Chebyshev orthogonal polynomials, the ill-posedness in the identification process can be improved and the stability of the electromagnetic load identification can be improved.

3. Polynomial Selection Technique for Improving the Identification Method

Using the polynomial selection technique [20], significant components are effectively selected from all possible polynomial terms with the aid of the error reduction ratio (ERR) and Gram–Schmidt orthogonalization. First, the Gramm–Schmidt orthogonal change is performed on each item in each cycle, then the error reduction ratio of each item is calculated, and the item with the largest error ratio is selected. By selecting a polynomial in each loop, until the error reduction ratio is less than the threshold, the selection is stopped and the selected item is significant.

3.1. Significant Selection of the Mode Shape Matrix. For a wind turbine rotor with N freedom degrees, there are N-order modal vectors on each equivalent concentrated load action point. n columns of $\mathbf{\Psi}$ shown in equation (9) is extracted from the N-order modal vectors. The mode shape matrix ϕ_o associated with the n equivalent concentrated load action point can be expressed as follows:

$$\phi_o = \begin{bmatrix} \phi_{11} & \phi_{12} & \cdots & \phi_{1N} \\ \phi_{21} & \phi_{22} & \cdots & \phi_{2N} \\ \vdots & \vdots & \ddots & \vdots \\ \phi_{n1} & \phi_{n2} & \cdots & \phi_{nN} \end{bmatrix} = [\,\phi_o(1) \;\cdots\; \phi_o(j) \;\cdots\; \phi_o(N)\,]. \tag{11}$$

Through the error reduction ratio ERR_o [20] of the mode shape matrix as equation (12), the n columns of the most significant mode shape matrix will be picked out from all the N columns of ϕ_{o} based on the polynomial selection technique.

$$\mathrm{ERR}_o = \frac{\sum_{j=1}^{n}\left(\sum_{j=1}^{n}F(j)\omega_o(j)/\sum_{j=1}^{n}\omega_o(j)\right)^2\omega_o^2(j)}{\sum_{j=1}^{n}(F(j))^2-\left(\sum_{j=1}^{n}F(j)\right)^2/n}, \quad (12)$$

where $\omega_o(j)=\varphi_o(j)-\sum_{o^{\#}=0}^{\nu_o-1}\sum_{j=1}^{\nu}\varphi_o(j)\omega_{o^{\#}}(j)/\sum_{j=1}^{\nu}\omega_{o^{\#}}^2(j)\,\omega_{o^{\#}}(j)$; $j=1,2,\cdots,n$; $n_o=1,2,\cdots,N$; $o^{\#}=0,\cdots,N-1$; N is the total amount of modes order; and n is the total amount of the equivalent concentrated load point.

3.2. Significant Selection of the Chebyshev Orthogonal Polynomial. The equivalent amplitude coefficients r_{ij} shown in equation (9) are related to Chebyshev orthogonal polynomials equivalent to the concentrated load action point. The n rows and m columns equivalent amplitude coefficients in the equation (10) are expressed as follows:

$$\mathbf{r}_i=\begin{bmatrix} r_{11} & r_{12} & \cdots & r_{1m}\\ r_{21} & r_{22} & \cdots & r_{2m}\\ \vdots & \vdots & \ddots & \vdots\\ r_{n1} & r_{n2} & \cdots & r_{nm}\end{bmatrix} = \begin{bmatrix} r_i(1) & \cdots & r_i(j) & \cdots & r_i(m)\end{bmatrix}, \quad (13)$$

$$\mathrm{ERR}_i = \frac{\sum_{j=1}^{n}\left(\sum_{j=1}^{n}\lambda(j)\nu_i(j)/\sum_{j=1}^{n}\nu_i(j)\right)^2\nu_i^2(j)}{\sum_{j=1}^{n}(\lambda(j))^2-\left(\sum_{j=1}^{n}\lambda(j)\right)^2/n}, \quad (14)$$

where $\nu_i(j)=r_i(j)-\sum_{i^{\#}=0}^{i-1}\sum_{j=1}^{n}r_i(j)\nu_{i^{\#}}(j)/\sum_{j=1}^{n}\nu_{i^{\#}}^2(j)\nu_{i^{\#}}(j)$; $j=1,2,\cdots,n$; $i=1,2,\cdots,m$; $i^{\#}=0,\cdots,m-1$; and m is the total amount of Chebyshev orthogonal polynomials' terms.

Through the error reduction ratio ERR_i of Chebyshev orthogonal polynomials reconstructing spatial distribution function as equation (14), the n columns' significant Chebyshev orthogonal polynomial will be picked out from all the m-term Chebyshev orthogonal polynomials based on the polynomial selection technique.

3.3. The Improved Electromagnetic Load Identification. Through the abovementioned procedure, the most significant mode shape matrix ϕ_o^* and equivalent amplitude coefficients $\mathbf{r}_i^*$ corresponding to significant Chebyshev orthogonal polynomials will be selected. Equation (10) can be rewritten as follows:

$$\boldsymbol{\lambda}=\boldsymbol{\varphi}_o^*\mathbf{r}_i^*\mathbf{a}. \quad (15)$$

The regularization method [26, 27] is usually used to eliminate ill-posed problem in identifying the coefficients $\mathbf{a}$ of Chebyshev orthogonal polynomials in equation (15) combined the known ratio $\boldsymbol{\lambda}$ together with the significant mode shape matrix ϕ_o^* and equivalent amplitude coefficients $\mathbf{r}_i^*$. To examine the identification accuracy, the correlation degree CC and the total error RE between the real $\mathbf{F}_r$ and identified load $\widetilde{\mathbf{F}}_r$ are defined as shown in the following equation:

$$\mathrm{CC}(\mathbf{F}_r,\widetilde{\mathbf{F}}_r)=\frac{\sum\sum[\mathbf{F}_r-E(\mathbf{F}_r)][\widetilde{\mathbf{F}}_r-E(\widetilde{\mathbf{F}}_r)]}{\left\|\widetilde{\mathbf{F}}_r-E(\widetilde{\mathbf{F}}_r)\right\|\left\|\mathbf{F}_r-E(\mathbf{F}_r)\right\|},$$
$$\mathrm{RE}(\mathbf{F}_r,\widetilde{\mathbf{F}}_r)=\frac{\left\|\widetilde{\mathbf{F}}_r-\mathbf{F}_r\right\|}{\left\|\mathbf{F}_r\right\|}. \quad (16)$$

4. Procedure of Obtaining the Electromagnetic Load

Generally speaking, the implementation details of the improved electromagnetic load identification with the aid of polynomial selection technique is described in Figure 2, and the identification procedure can be described as follows:

Step 1: with known $\mathbf{M}$, $\mathbf{K}$, and $\mathbf{C}$ of the wind turbine rotor, specify the displacement measured node and get the corresponding displacement vector $\mathbf{q}$.

Step 2: combine measured response $\mathbf{q}$ together with the Green's function matrix $\mathbf{G}$ into the centralized dynamic load identification method to identify the equivalent dynamic load $\mathbf{F}$ on the corresponding concentrated load node.

Step 3: gain the significant mode shape matrix ϕ_o^* from the mode shape matrix ϕ_o shown in equation (11) using equation (12) based on the polynomial structure selection technique. Also, combine them with the equivalent dynamic load $\mathbf{F}$ into the modal transformation $\mathbf{p}^d=\boldsymbol{\Phi}^T\mathbf{F}$ to calculate the modal electromagnetic load $\mathbf{p}^d$ and denote an assumed order modal load $s(t)$ as the time-history function.

Step 4: gain the corresponding coefficient regarding $s(t)$ as the ratio λ_j. Combine them with equivalent amplitude coefficients $\mathbf{r}_i$ shown in equation (13) using equation (14) into polynomial structure selection technique to gain the significant Chebyshev orthogonal polynomial.

Step 5: compute the corresponding coefficient a_i of the significant Chebyshev orthogonal polynomial through the regularization method using the obtained ratio $\boldsymbol{\lambda}$ with the significant mode shape matrix ϕ_o^* and equivalent amplitude coefficients $\mathbf{r}_{\mathrm{i}}^*$. Obtain fitting spatial function $f(z)$.

Step 6: reconstruct the electromagnetic load centering on $s(t)$ and $f(z)$.

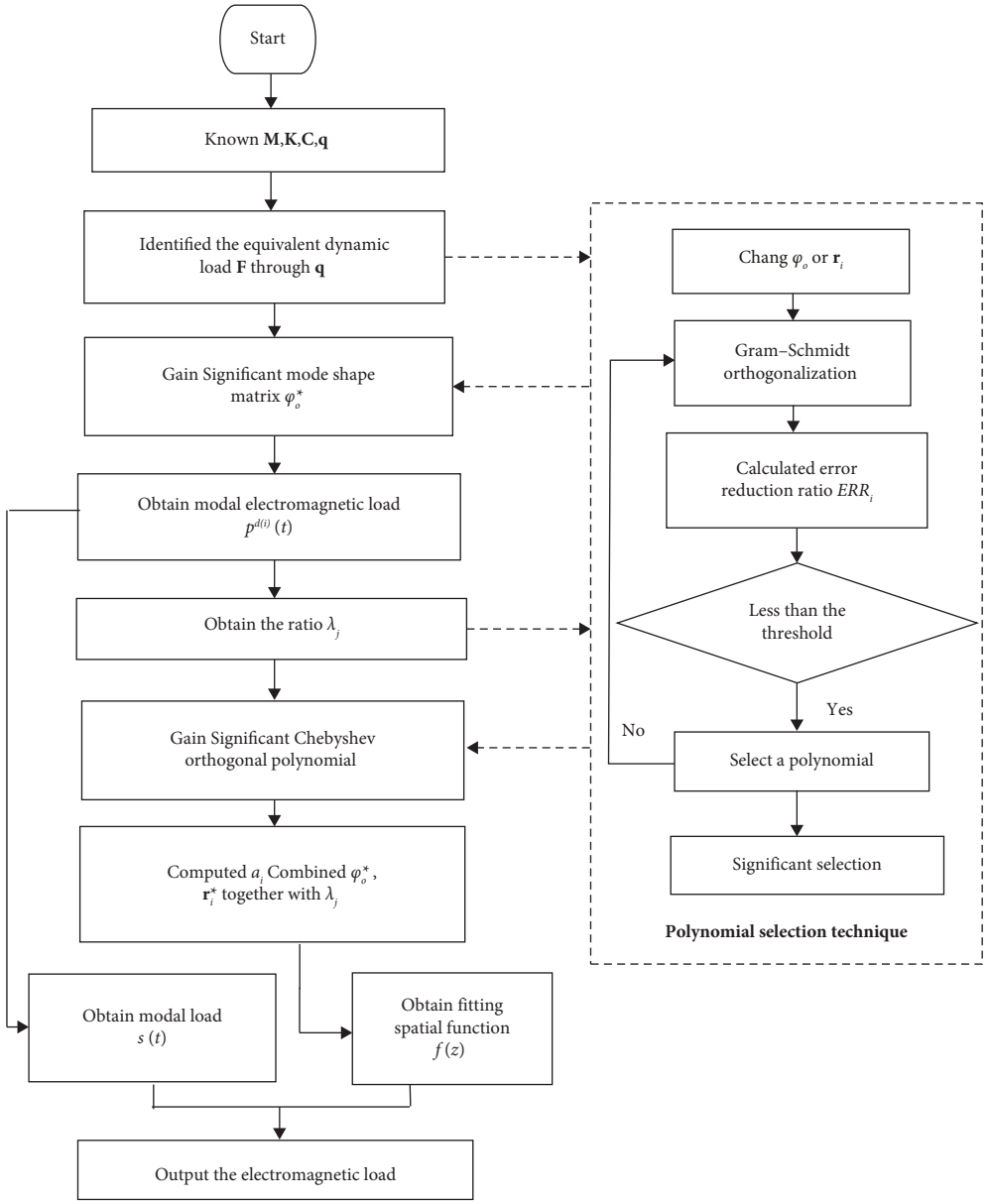

Figure 2: Identification flowchart.

5. Numerical Examples

The numerical example (Table 1 and Figure 3) coming from the literature [19] is given to examine the proposed identification method. The electromagnetic loads acting vertically along the axis 335 mm–495 mm is selected as $(z) = (z-3)(z-2), z \in [335, 495]$mm, and $l(t) = 3\sin(60\pi t) + 2\sin(90\pi t), t \in [0, 0.1]s$. The six terms of Chebyshev orthogonal polynomials ($R_1(z) = 1, R_2(z) = z, R_3(z) = 2z^2 - 1, R_4(z) = 4z^3 - 3z,$ $R_5(z) = 8z^4 - 8z^2 - 1,$ and $R_6(z) = 16z^5 - 20z^3 + 5z$) are discretely equivalented into six concentrated load nodes 12, 13, 14, 15, and 16 corresponding to the shaft length of 335 mm, 375 mm, 415 mm, 455 mm, and 495 mm. $z = 2(z - z_0)/(z_1 - z_0) - 1$ is applied to transform the interval $[z_0, z_1]$ into $[-1, 1]$. The equivalent amplitude coefficients r_{ij} are shown in Table 2.

5.1. Identification Based on the Measured Displacement Response. The displacement responses in the time domain at five measuring points 1, 2, 5, 28, and 30 are obtained using assumed loads through the finite element method, as shown in Figure 4. The displacement responses are used as measured displacement responses **q**. The equivalent concentrated dynamic load **F** acting on the five corresponding concentrated load nodes 12, 13, 14, 15, and 16 have been identified, as shown in Figure 5. As shown in Figure 3, the rotor model is divided into 34 nodes with 136 order modes, and the 39th, 80th, 81th, 105th, and 117th order relative effective modal shape are picked out from the 136 order modes corresponding to five concentrated load nodes 12, 13, 14, 15, and 16 through the polynomial selection technique. Then, the significant mode shape matrix ϕ_o^* can be reconstructed based on the five-order effective modal shape

Table 1: Stiffness and damping coefficients of bearings.

Bearings	Stiffness coefficients ($MN \cdot m^{-1}$)				Damping coefficients ($KN \cdot s \cdot m^{-1}$)			
	K_{xx}	K_{xy}	K_{yx}	K_{yy}	C_{xx}	C_{xy}	C_{yx}	C_{yy}
Left	46.355	83.40	−64.334	41.270	70.277	71.629	71.629	88.570
Right	13.376	29.160	−21.780	8.361	69.673	19.977	19.977	79.934

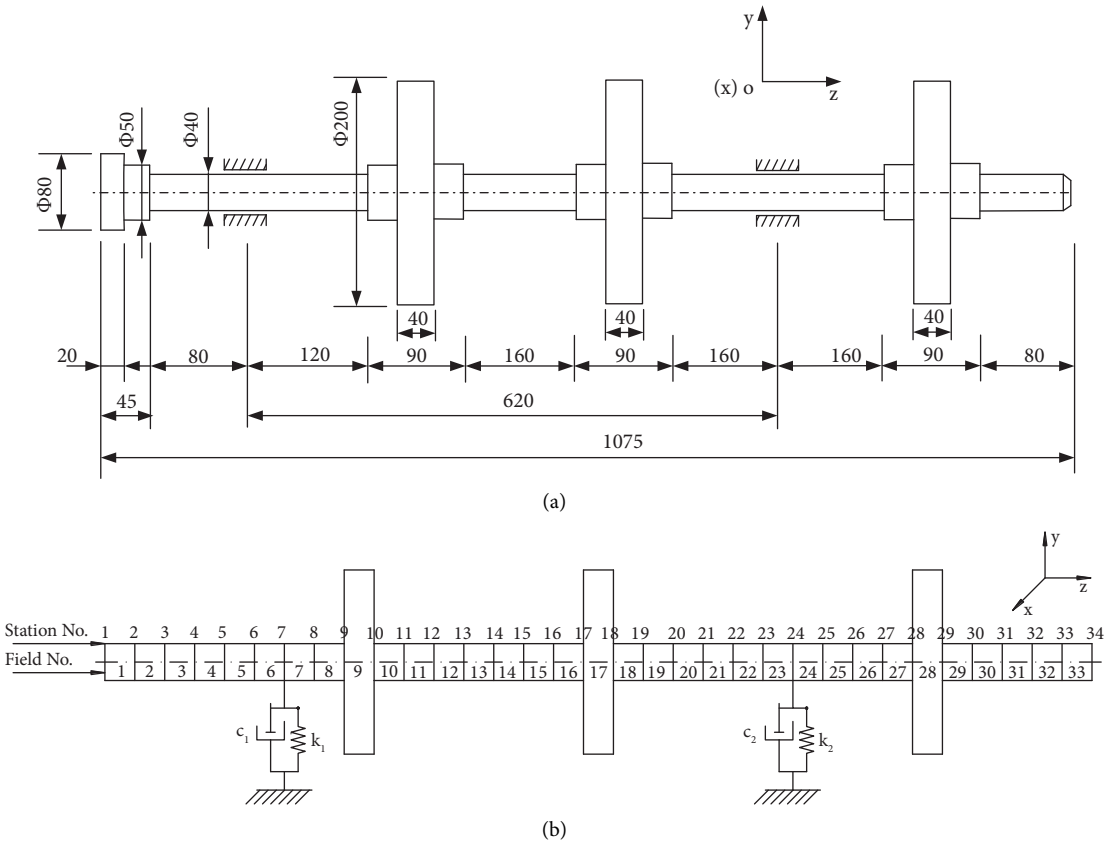

Figure 3: Rotor system model. (a) The structural parametric model. (b) The TMM model.

Table 2: Equivalent amplitude coefficient.

Load nodes	Chebyshev orthogonal polynomial					
	R1	R2	R3	R4	R5	R6
12	1	−1	1	−1	−1	−1
13	2	−1	−1	2	−5	1
14	2	−0	−2	0	−2	0
15	2	−1	−1	−2	−5	1
16	1	1	1	1	−1	1

mentioned above. Combine ϕ_o^* together with the equivalent concentrated dynamic load shown in Figure 5 into the modal transformation to calculate the 39th, 80th, 81th, 105th, and 117th effective modal electromagnetic load, as shown in Figure 6. The coefficient $C2 = -0.1992$ in the proposed method is different from the coefficient $C1 = 0.3997$ in literature [19] due to the different significant mode shape matrix ϕ_o^* corresponding to five concentrated load nodes 12, 13, 14, 15, and 16. The significant mode shape matrix ϕ_o^* in literature [19] is reconstructed coming from directly selecting the 12th, 13th, 14th, 15th, and 16th order relative modal shapes instead of the 39th, 80th, 81th, 105th, and 117th order relative effective modal shapes by the polynomial selection technique. Both methods can accurately reconstruct the time history, which shows that the selection of modal shape does not affect the time-history function identification.

The ratio between the modal loads on equivalent concentrated load nodes 12, 13, 14, 15, and 16 with a 39th order modal load $s(t)$ is $\lambda_1 = 1$, $\lambda_2 = -0.308$, $\lambda_3 = -5.193$,

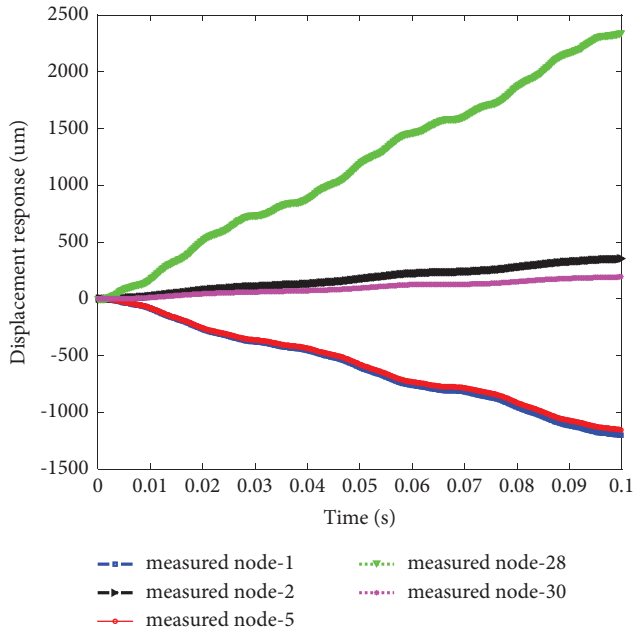

Figure 4: Measured displacement response.

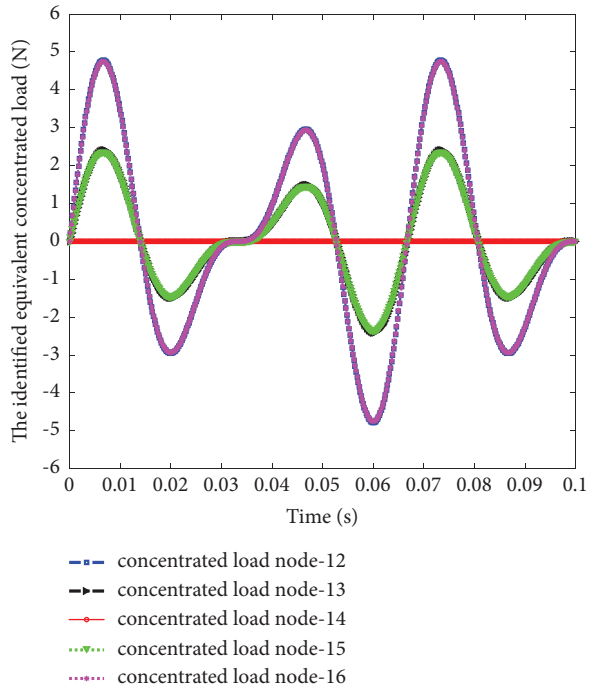

Figure 5: The identified equivalent concentrated load.

$\lambda_4 = -1.065$, and $\lambda_5 = -10.741$, respectively (see the 4th row of Table 3). Combine these ratios together with equivalent amplitude coefficients shown in Table 2 into the polynomial structure selection technique to gain the significant Chebyshev orthogonal polynomial. The first and third of the six term Chebyshev orthogonal polynomial are picked out as the significant Chebyshev orthogonal polynomial. According to equation (15), the corresponding coefficient of the significant Chebyshev orthogonal polynomial through the regularization method is computed as $a_1 = -0.099$, $a_2 = 0$, $a_3 = -0.1$, $a_4 = 0$, $a_5 = 0$, and $a_6 = 0$ (see the 4th row of Table 3). Compared with the identified and real spatial distribution function (see Figure 7), they have the same form and different coefficients $1/c2$. So, the spatial distribution function identification method is feasible. Furthermore, the 4th row of Table 4 shows that the correlation coefficient and the total relative error are 1 and 0.86, respectively, which is smaller than the 0.9979 and 4.87% from literature [19],

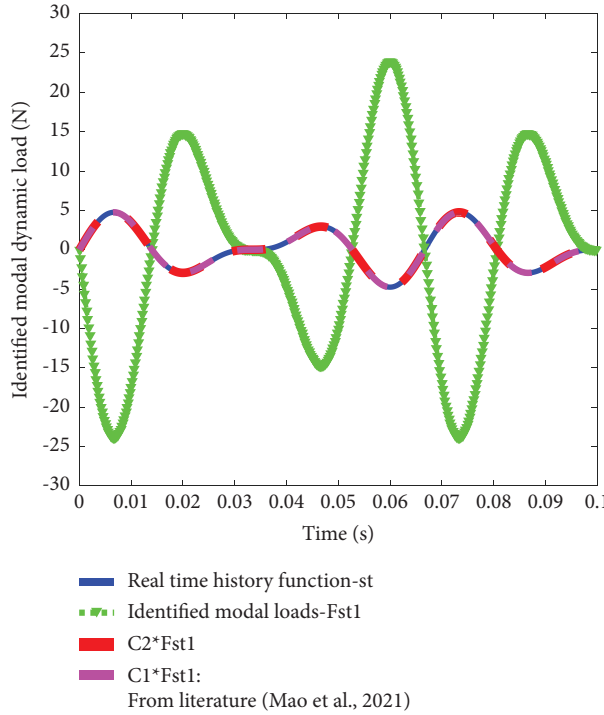

Figure 6: Identified modal dynamic load.

Table 3: Modal load relative ratio and coefficients of each basis function.

Noise levels	Modal load relative ratio					Chebyshev orthogonal polynomial coefficients					
	λ_1	λ_2	λ_3	λ_4	λ_5	a_1	a_2	a_3	a_4	a_5	a_6
Literature [19]	1	−5.042	−0.950	−4.854	0.6953	0.202	−0.009	0.197	0.007	—	—
0% (I)	1	−0.308	−5.193	−1.065	−10.741	−0.106	−0.019	−0.076	−0.199	—	—
0% (II)	1	1.090	−0.201	−1.049	−0.147	0.043	0	0.044	0	0	0
0% (III)	1	−0.308	−5.193	−1.065	−10.741	−0.099	0	−0.1	0	0	0
3%	1	0.462	−9.661	−2.908	−5.196	−0.099	0	−0.1	0	0	0
5%	1	−0.056	−5.206	0.389	−9.676	−0.099	0	−0.101	0	0	0
10%	1	0.609	−5.137	0.109	2.391	−0.103	0	−0.098	0	0	0

which shows that the selection of the significant Chebyshev orthogonal polynomial is effective to the spatial characteristic identification.

We reconstructed the electromagnetic load centering on the present time-history function (see the green curve in Figure 6) and spatial distribution function (see the green curve in Figure 7). The identified and real electromagnetic load is shown in Figure 8, and the detailed results are shown in the 4th row of Table 4. Apparently, the error between them fluctuates between −0.04 N and 0.03 N, and its recognition error is smaller than the fluctuation between −0.2 N and 0.2 N, which shows that the identified electromagnetic load according to the proposed method is more accurate.

To further verify the electromagnetic load identification accuracy due to the selection of the significant mode shape matrix and the Chebyshev orthogonal polynomial, we compared with the following three types of programs: (I) only selecting the significant mode shape matrix; (II) only selecting the significant Chebyshev orthogonal polynomial; and (III) selecting both the significant mode shape matrix and the Chebyshev orthogonal polynomial (the proposed method). The identification errors of the three programs are shown in Figure 9, and the detailed results are shown in Tables 3 and 4 (see the 2nd, 3rd, and 4th row of Tables 3 and 4). Figure 9 shows that (III) has a smaller error compared with (I) and (II); the proposed method in the paper has a higher accuracy than the other programs where only the effective mode or Chebyshev polynomial are selected by polynomial selection techniques. It can find that selecting the significant mode shape matrix is important to the electromagnetic load identification accuracy. It directly affects the fitting accuracy of the spatial distribution function through the ratio $\boldsymbol{\lambda}$ which will cause ill-posed problem in identifying the coefficients $\mathbf{a}$.

5.2. Identification Based on the Measured Displacement Response with Noise. In the section, three different Gaussian noises of 3%, 5%, and 10% are used to check the robustness. Corresponding results are, respectively, shown in the 5th, 6th, and 7th row of Tables 3 and 4 and Figure 10. The results

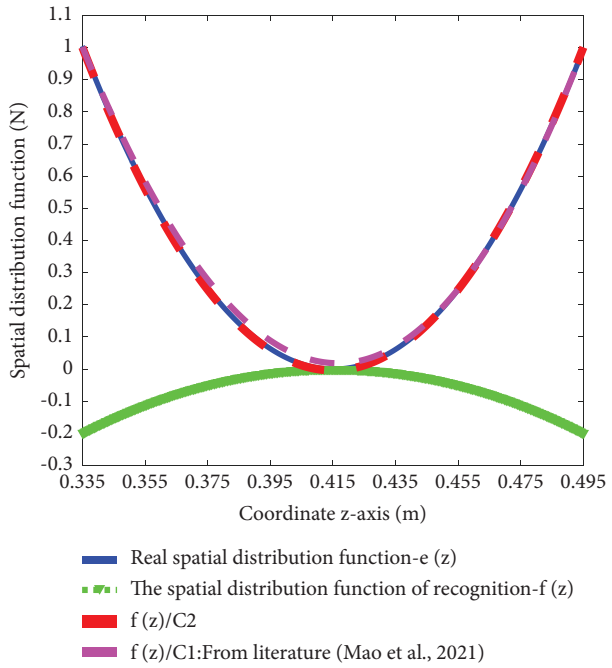

Figure 7: Identified spatial distribution function.

Table 4: Comparison of identified and real results.

Noise levels	Correlation degree $CC(\mathbf{F}_r, \tilde{\mathbf{F}}_r)$			Total error $RE(\mathbf{F}_r, \tilde{\mathbf{F}}_r)$		
	$l(t), s(t)/C2$	$e(z), C2f(z)$	$\mathbf{F}(e,t), \tilde{\mathbf{F}}(e,t)$	$l(t), s(t)/C2$, (%)	$e(z), C2f(z)$ (%)	$\mathbf{F}(e,t), \tilde{\mathbf{F}}(e,t)$ (%)
Literature [19]	1	0.9979	0.9989	0.01	4.87	4.87
0% (I)	1	0.9335	0.9592	0.01	29.81	29.81
0% (II)	1	1	1	0.02	0.98	0.98
0% (III)	1	1	1	0.01	0.86	0.86
3%	0.9998	1	0.9998	1.99	1.07	2.23
5%	0.9998	1	0.9998	1.89	1.12	2.17
10%	0.9999	0.9947	0.9971	1.49	7.87	8.01

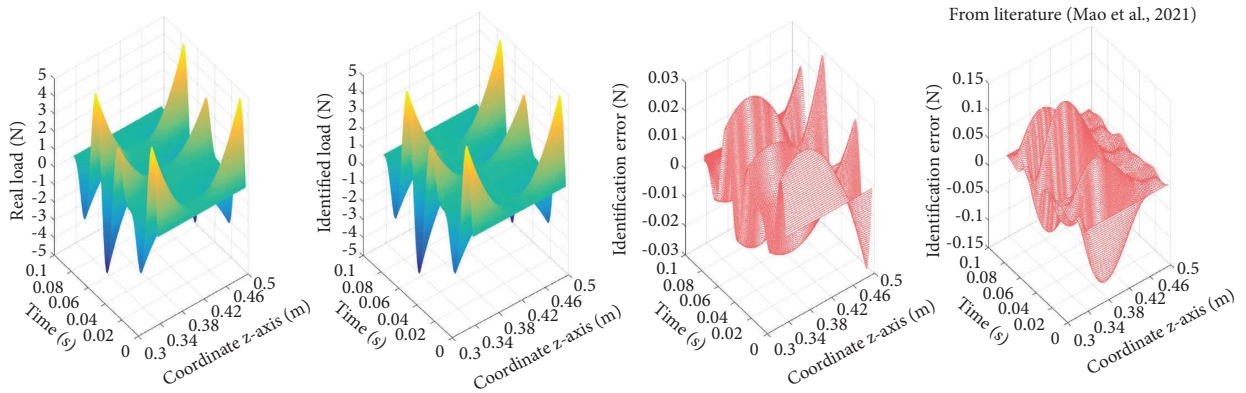

Figure 8: Identified electromagnetic loads.

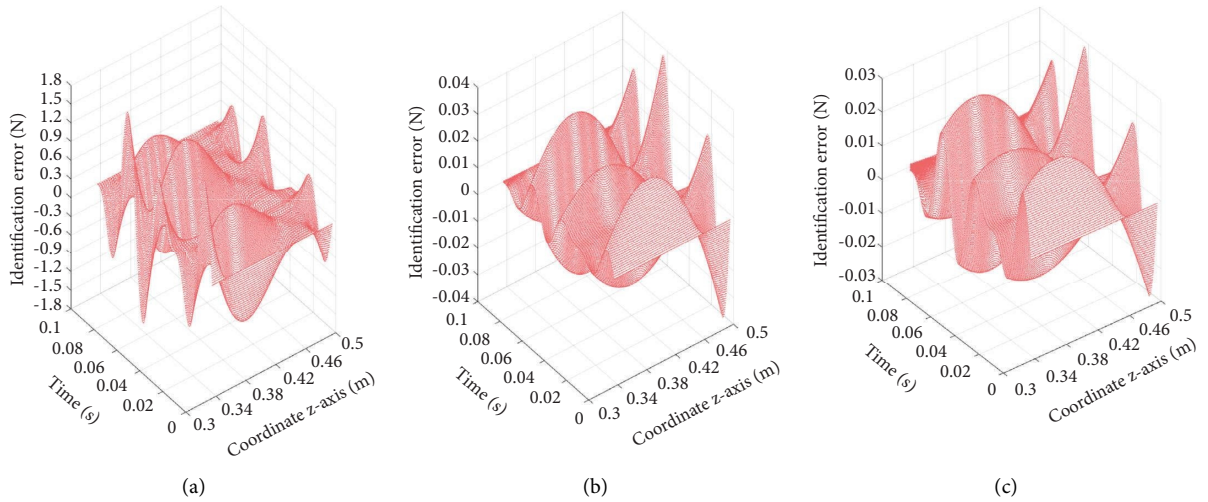

Figure 9: Comparison of identification errors under three types of programs. (a) Only valid modes are selected. (b) Only valid Chebyshev polynomials are selected. (c) Effective modes and Chebyshev polynomials are selected.

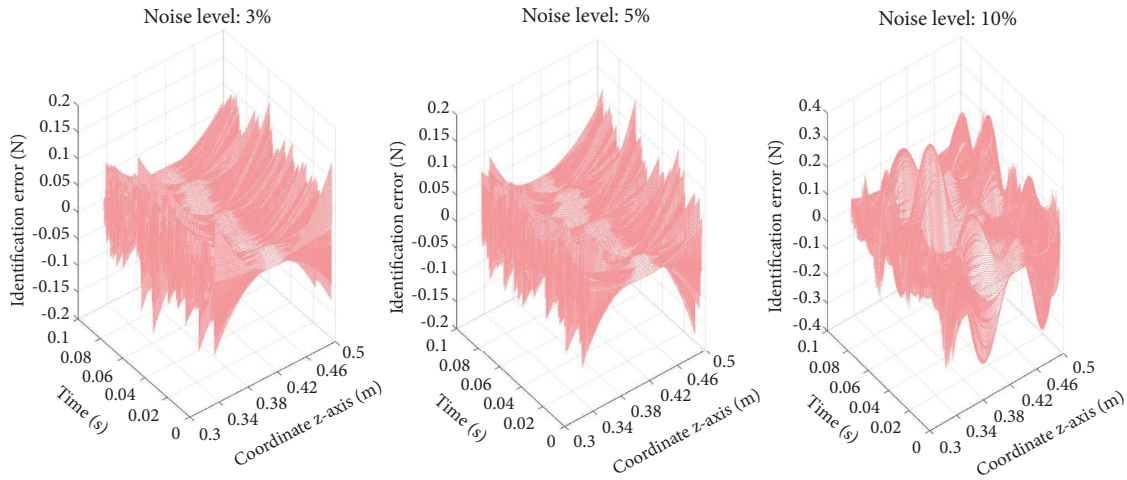

Figure 10: Identification errors of different noise levels.

of 0.9998, 0.9998, and 0.9971 and 2.23%, 2.17%, and 8.01% (see Table 4) show that the improved method is robust when actual measurement noises are considered below 5%.

6. Conclusion

In the process of identifying the electromagnetic load, a polynomial selection technique for the significant mode shape matrix and the Chebyshev orthogonal polynomial is proposed in the present paper. A numerical example is studied and used to illustrate the feasibility and validity of the improved method. The following novelties and conclusions can be derived from this study:

(1) This method demonstrates the similarity between the time-history function and the modal loads. The selection of the modal shape has a little effect on the time-history function identification.

(2) The polynomial selection technique helped to pick out the significant mode shape matrix and the Chebyshev orthogonal polynomial, and the proposed method in the paper has a higher accuracy than the other programs where only the effective mode or Chebyshev polynomial are selected by polynomial selection techniques. Selecting the significant mode shape matrix does not affect the accuracy of time-history function identification but has a great influence on the accuracy of spatial distribution function reconstruction.

(3) The identification results according to the measured displacement response with noise substantiate the effectiveness and robustness of the proposed method.

Data Availability

The data supporting the conclusion of the article are shown in the relevant figures and tables in the article.

Conflicts of Interest

The authors declare that they have no conflicts of interest.

Acknowledgments

This work was supported by the National Natural Science Foundation of China (grant nos. 52375244 and 51775180), the Hunan Provincial Natural Science Foundation of China (grant nos. 2023JJ30192 and 2021JJ50101), the Scientific Research Foundation of Hunan Provincial Education Department (grant no. 21A0457), the Xiangtan Science and Technology Plan Key Project (grant no. GX-ZD20221008), and the Postgraduate Scientific Research Innovation Project of Hunan Province (grant no. CX20221298).

References

[1] J. M. Du and Y. Li, "Analysis on the variation laws of electromagnetic force wave and vibration response of squirrel-cage induction motor under rotor eccentricity," *Electronics*, vol. 12, no. 6, p. 1295, 2023.

[2] Z. F. Wang, W. Tian, and W. X. Zhao, "Magnet slotting design to reduce high order electromagnetic force and vibration of permanent magnet motor," *Energies*, vol. 15, no. 22, p. 8684, 2022.

[3] X. Li, Z. X. Deng, T. Q. Liu, and S. E. Zhao, "Analytical representation and characteristics optimization for radial electromagnetic force of the switched reluctance motor under airgap eccentricity," *Proceedings of the Institution of Mechanical Engineers- Part C: Journal of Mechanical Engineering Science*, vol. 236, no. 14, pp. 7629–7640, 2022.

[4] Y. C. Hu, X. Wang, W. Y. Li, J. H. Hu, S. W. Chen, and D. Wang, "Influence of static air-gap eccentricity on the vibration of an asymmetric PMSM rotor," *Journal of Vibration and Shock*, vol. 42, no. 12, pp. 164–171, 2023.

[5] J. T. Yin, Z. L. He, L. Liu, and Z. H. Peng, "Air gap eccentric analysis and fault detection of traction motor," *Journal of Engineering and Applied Science*, vol. 70, no. 1, p. 62, 2023.

[6] Z. X. Deng, X. Li, X. Q. Li, S. E. Zhao, and H. B. Wei, "Mechanism analysis and optimum control of negative airgap eccentricity effect for in-wheel switched reluctance motor driving system," *Nonlinear Dynamics*, vol. 111, no. 10, pp. 9075–9093, 2023.

[7] Y. Fan, H. N. Wang, L. T. Xie, N. Hu, and J. G. Yang, "Armature structure optimization of annular multipole solenoid valves based on electromagnetic force distribution," *Actuators*, vol. 12, no. 2, p. 54, 2023.

[8] Z. Li, L. B. Liu, P. J. Wang et al., "Modeling and analysis of radial electromagnetic force and vibration characteristics based on deflection dual-stator switched reluctance generator," *Micromachines*, vol. 13, no. 9, p. 1494, 2022.

[9] Z. P. Wu, S. G. Zuo, Z. Y. Huang, X. R. Hu, S. Y. Chen, and C. Liu, "Modelling, calculation and analysis of electromagnetic force and vibroacoustic behavior of integer-slot permanent magnet synchronous motor considering current harmonics," *Journal of Vibration Engineering and Technologies*, vol. 10, no. 3, pp. 1135–1152, 2022.

[10] L. Wang, Y. R. Liu, and Y. S. Liu, "An inverse method for distributed dynamic load identification of structures with interval uncertainties," *Advances in Engineering Software*, vol. 131, pp. 77–89, 2019.

[11] L. Wang, H. Y. Xu, and Y. R. Liu, "A novel dynamic load identification approach for multi-source uncertain structures based on the set-theoretical wavelet transform and layered noise reduction," *Structures*, vol. 51, pp. 91–104, 2023.

[12] C. Zhang, Y. Z. Fu, Y. D. Li, and J. X. Li, "Identification of aircraft skin distributed dynamic load based on strain modal method," *Equipment Environmental Engineering*, vol. 17, no. 9, pp. 113–117, 2020.

[13] D. Wei, D. S. Li, T. Jiang, P. Lyu, and X. F. Song, "Load identification of a 2.5 MW wind turbine tower using Kalman filtering techniques and BDS data," *Engineering Structures*, vol. 281, p. 115763, 2023.

[14] S. Y. Luo, J. H. Jiang, F. Zhang, and M. S. Mohamed, "Distributed dynamic load identification of beam structures using a bayesian method," *Applied Sciences*, vol. 13, no. 4, p. 2537, 2023.

[15] S. Y. Luo, J. H. Jiang, and F. Zhang, "Experimental dynam- ic calibration method of distributed dynamic loads identification in frequency-domain," *Journal of Vibration Engineering*, vol. 36, no. 3, pp. 706–717, 2023.

[16] Y. R. Liu, L. Wang, M. Li, and Z. Wu, "A distributed dynamic load identification method based on the hierarchical-clustering-oriented radial basis function framework using acceleration signals under convex-fuzzy hybrid uncertainties," *Mechanical Systems and Signal Processing*, vol. 172, Article ID 108935, 2022.

[17] K. Li, J. Liu, X. Han, X. S. Sun, and C. Jiang, "A novel approach for distributed dynamic load reconstruction by space–time domain decoupling," *Journal of Sound and Vibration*, vol. 348, pp. 137–148, 2015.

[18] J. H. Jiang, H. F. Kong, H. J. Yang, and J. D. Chen, "One identification method of distributed dynamic load based on modal coordinate transformation for thin plate structure," *International Journal of Computational Methods*, vol. 18, no. 7, pp. 1–18, 2021.

[19] W. G. Mao, J. H. Li, C. L. Hu, and S. X. Pei, "A novel approach for identifying electromagnetic space–time coupling load of wind turbine," in *Proceedings of the International Conference on Mechanical Design*, pp. 125–137, Springer, Huzhou, China, August, 2021.

[20] K. Li, J. Liu, X. Han, C. Jiang, and D. Q. Zhang, "Distributed dynamic load identification based on shape function method and polynomial selection technique," *Inverse Problems in Science and Engineering*, vol. 25, no. 9, pp. 1323–1342, 2016.

[21] Q. Lei, Y. Yuan, and J. J. Du, "Research on dynamic characteristics of high-speed air floating motorized spindle rotor in flying cutter milling," *Journal of Mechanical Engineering*, vol. 57, no. 13, pp. 45–54, 2021.

[22] J. S. Hwang, A. Kareem, and W. J. Kim, "Estimation of modal loads using structural response," *Journal of Sound and Vibration*, vol. 326, no. 3-5, pp. 522–539, 2009.

[23] J. H. Jiang, N. S. Shen, M. S. Mohamed, and F. Zhang, "Dynamic load identification of unspecified metal structures by measuring their response," *Metals*, vol. 12, no. 11, p. 1872, 2022.

[24] F. Li, H. F. Li, H. Zhao, and Y. Zhou, "A dimension-reduction based Chebyshev polynomial method for uncertainty analysis in composite corrugated sandwich structures," *Journal of Composite Materials*, vol. 56, no. 12, pp. 1891–1900, 2022.

[25] H. Yang, N. Li, and B. S. Xu, "Calculation for equivalent nodal force of prestress in 20 nodes isoparametric element," *Applied Mechanics and Materials*, vol. 142, pp. 129–133, 2011.

[26] L. S. Yang, S. F. Xue, X. G. Zhang, and W. Yao, "A regularization method for solving dynamic problems with singular configuration," *Proceedings of the Institution of Mechanical Engineers- Part K: Journal of Multi-body Dynamics*, vol. 236, no. 1, pp. 3–14, 2022.

[27] J. Jiang, H. Z. Tang, M. S. Mohamed, S. Y. Luo, and J. D. Chen, "Augmented tikhonov regularization method for dynamic load identification," *Applied Sciences*, vol. 10, no. 18, p. 6348, 2020.